Exploring Galactic Cosmic-Ray Acceelerators with Ultra-High Energy Gamma-Rays

Pulsar Halos as leptonic orgin of DGE: Implcations from LHAASO and IceCube

Kai Yan
School of Astronomy and Space Science
Nanjing University

Collaborators: Ruo-Yu Liu, Rui Zhang, Chao-Ming Li, Qiang Yuan, and Xiang-Yu Wang

Galactic Diffuse Gamma-ray Background (DGE)

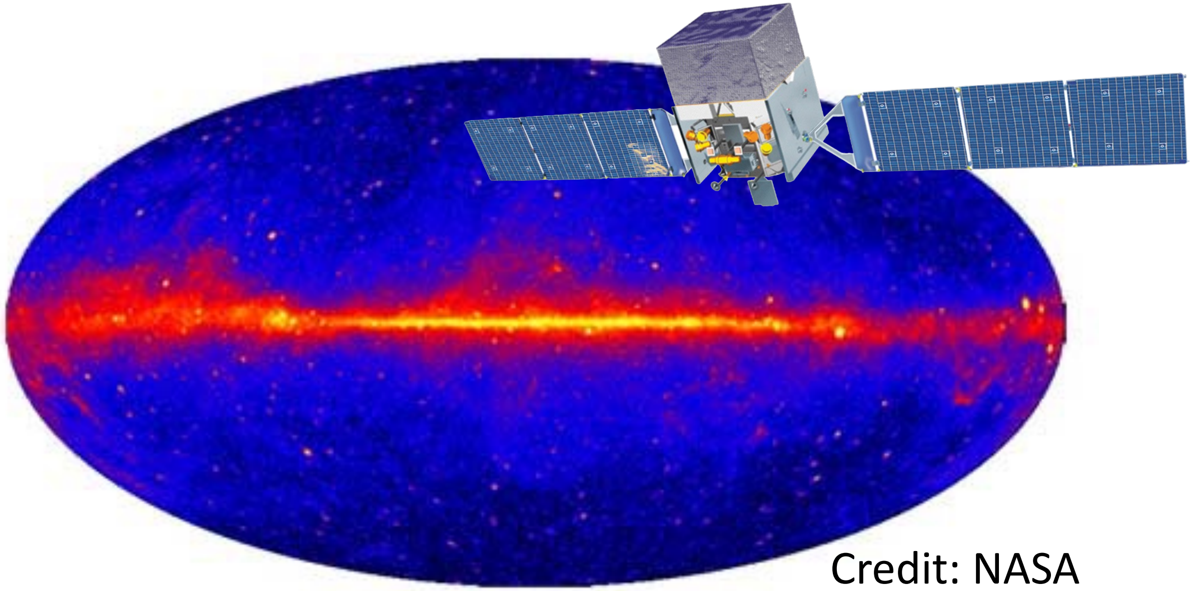

Credit: NASA

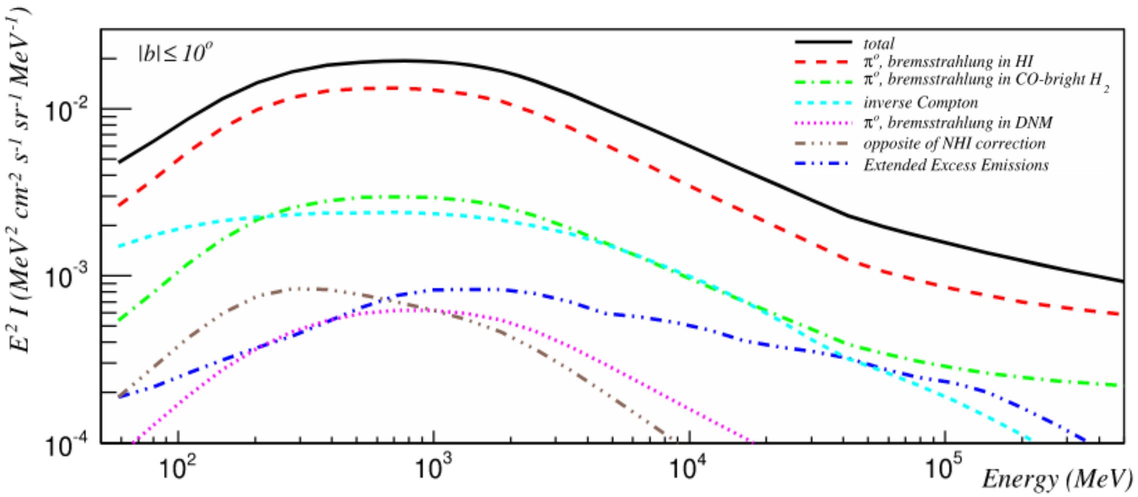

Fermi-LAT Collaboration 2016, ApJS

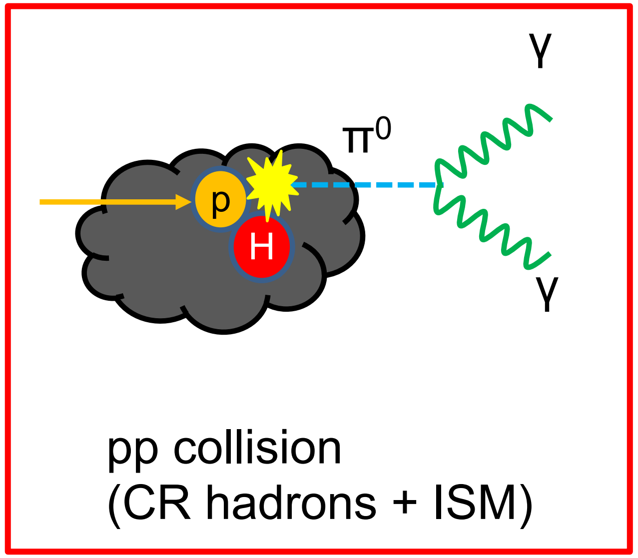

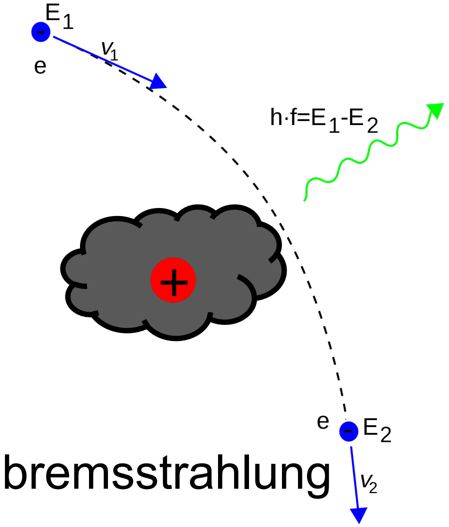

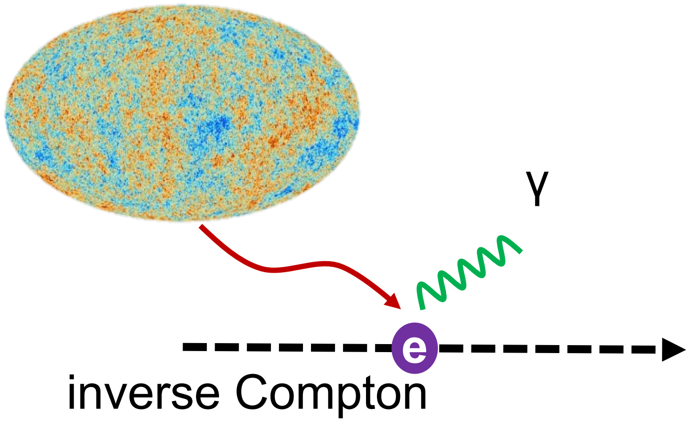

DGE at TeV-PeV band

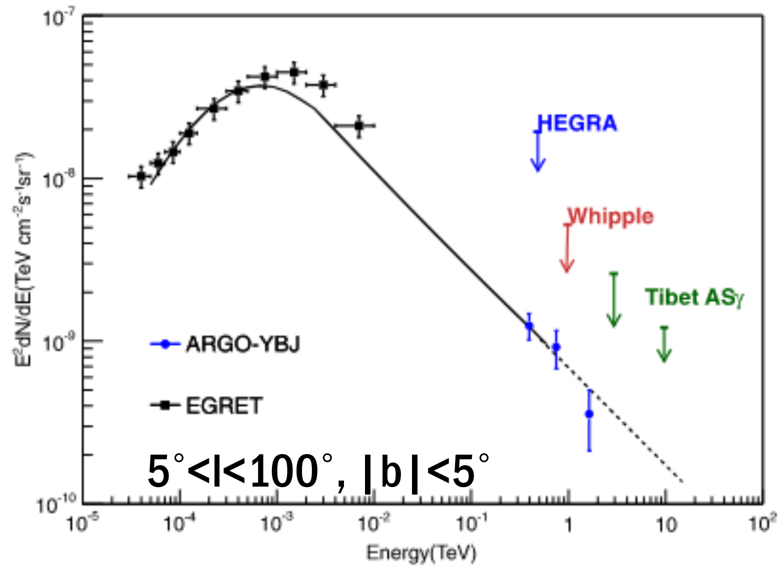

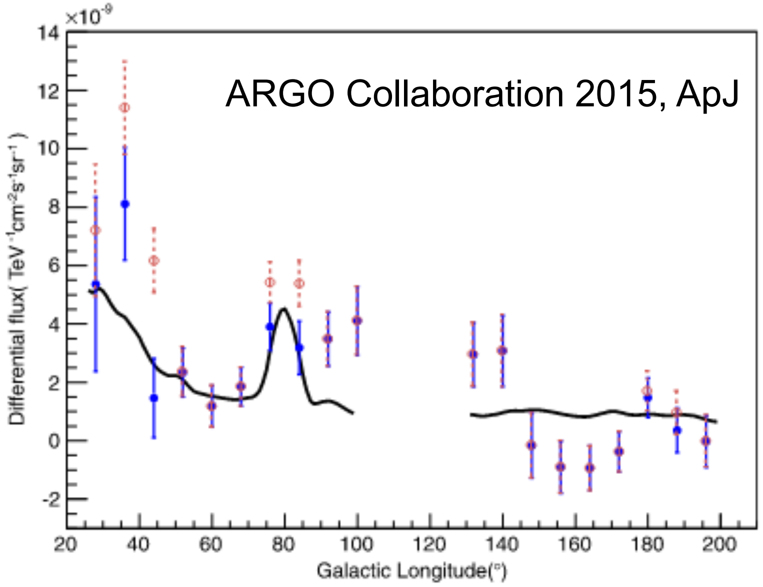

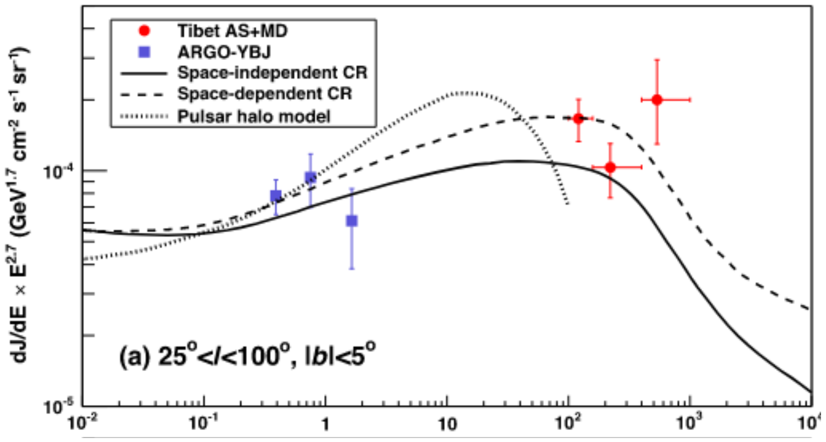

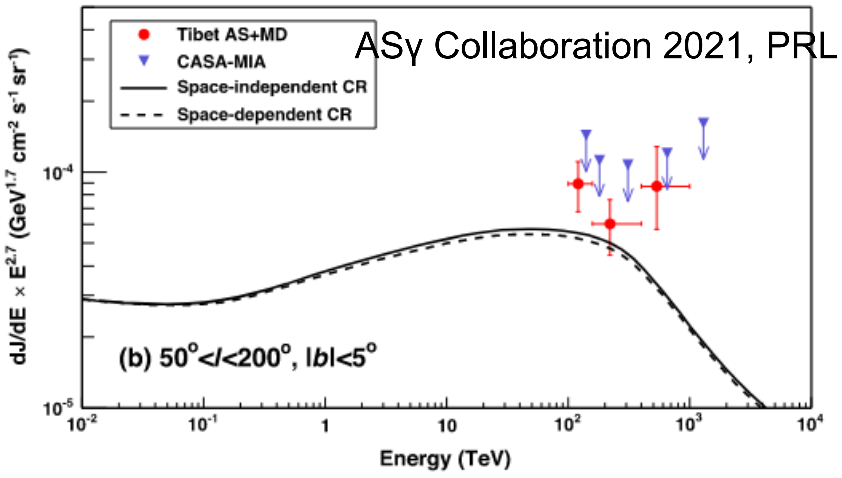

Contribution of Extended Sources and Unresolved Sources

Diffuse Emission = All Emission - Identified Sources (point/extended)

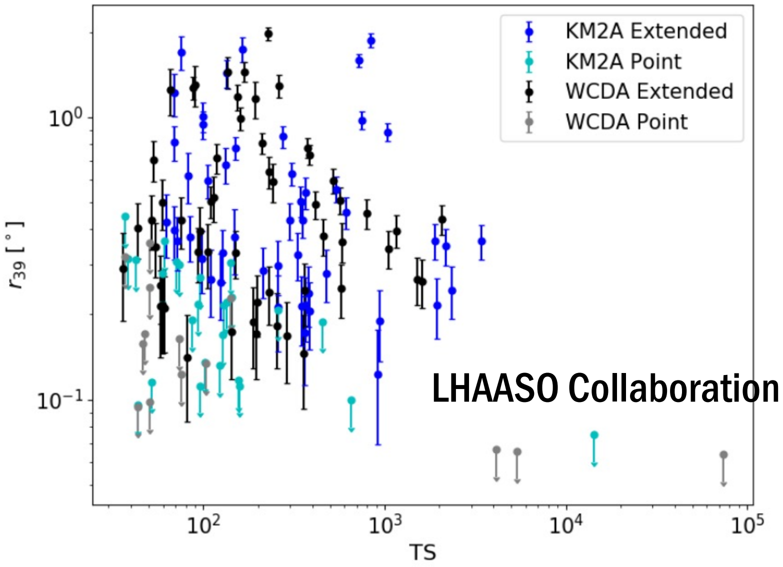

LHAASO Collaboration 2023, ApJS

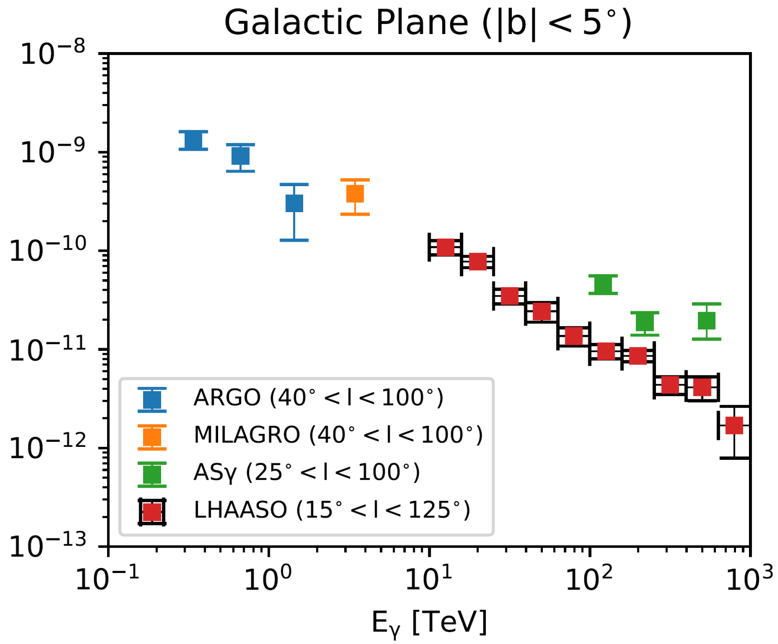

2D Gaussian Profile
σ=0.5 deg
0.5 deg ~ 39% containment of total flux

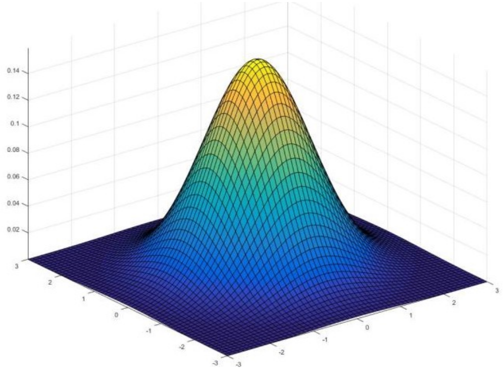

LHAASO' latest measurements

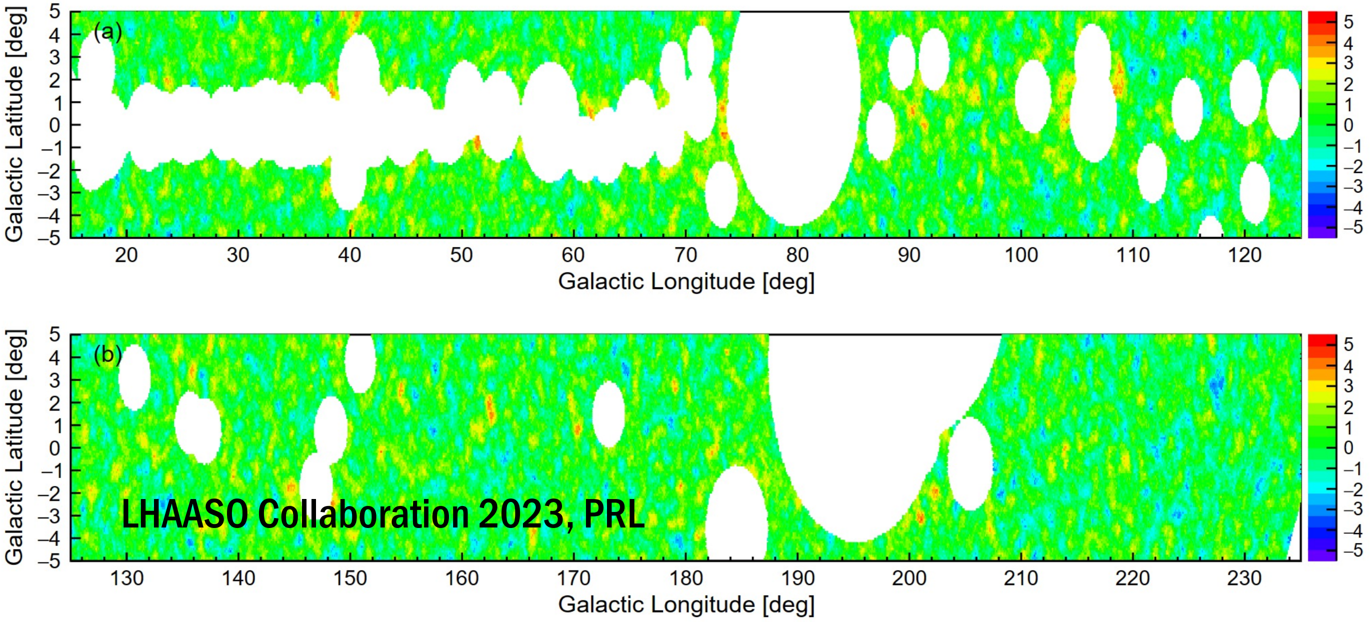

LHAASO Collaboration 2023, PRL

$$R_{\text{mask}} = n \cdot \sigma \qquad \sigma = \sqrt{\sigma_{\text{psf}}^2 + \sigma_{\text{ext}}^2} \qquad n = 2.5$$

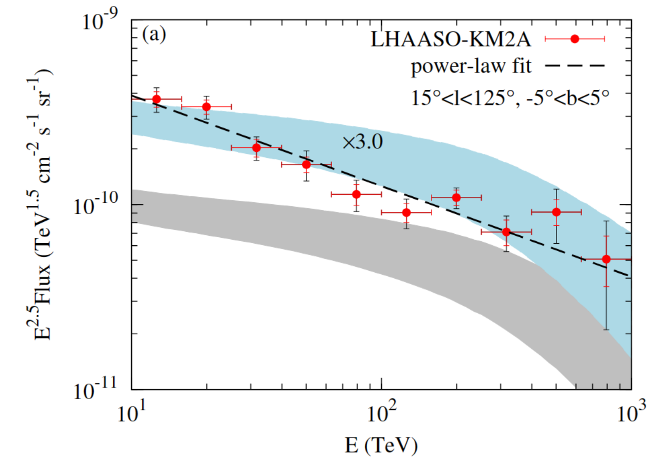

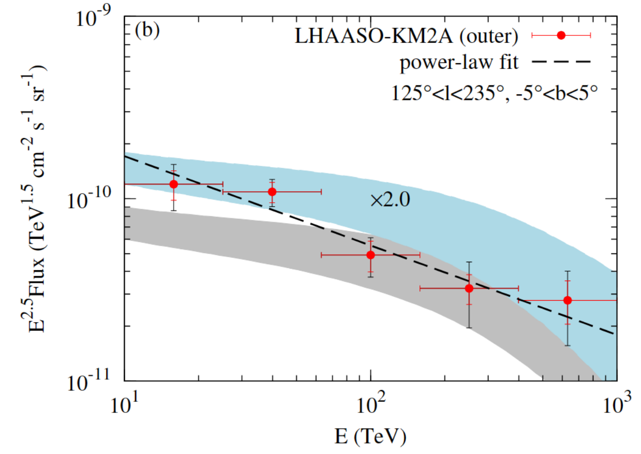

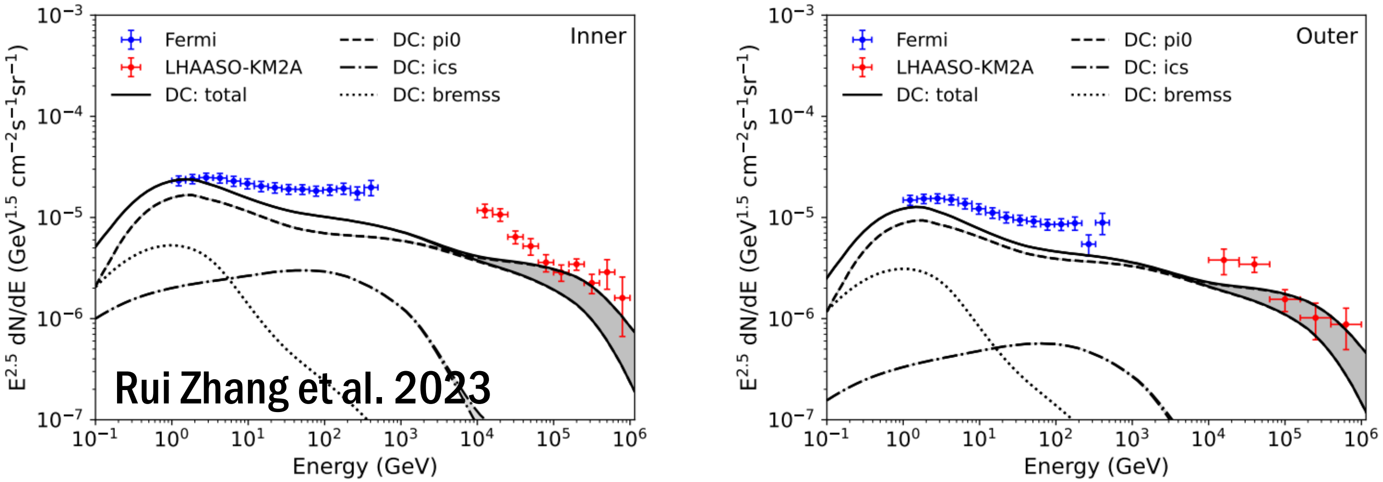

Rui Zhang et al. 2023

Local CR density x Gas column density

- more complex CR transport
- additional contribution other than CRs

Neutrino detection from our Galaxy with a significance over 4σ

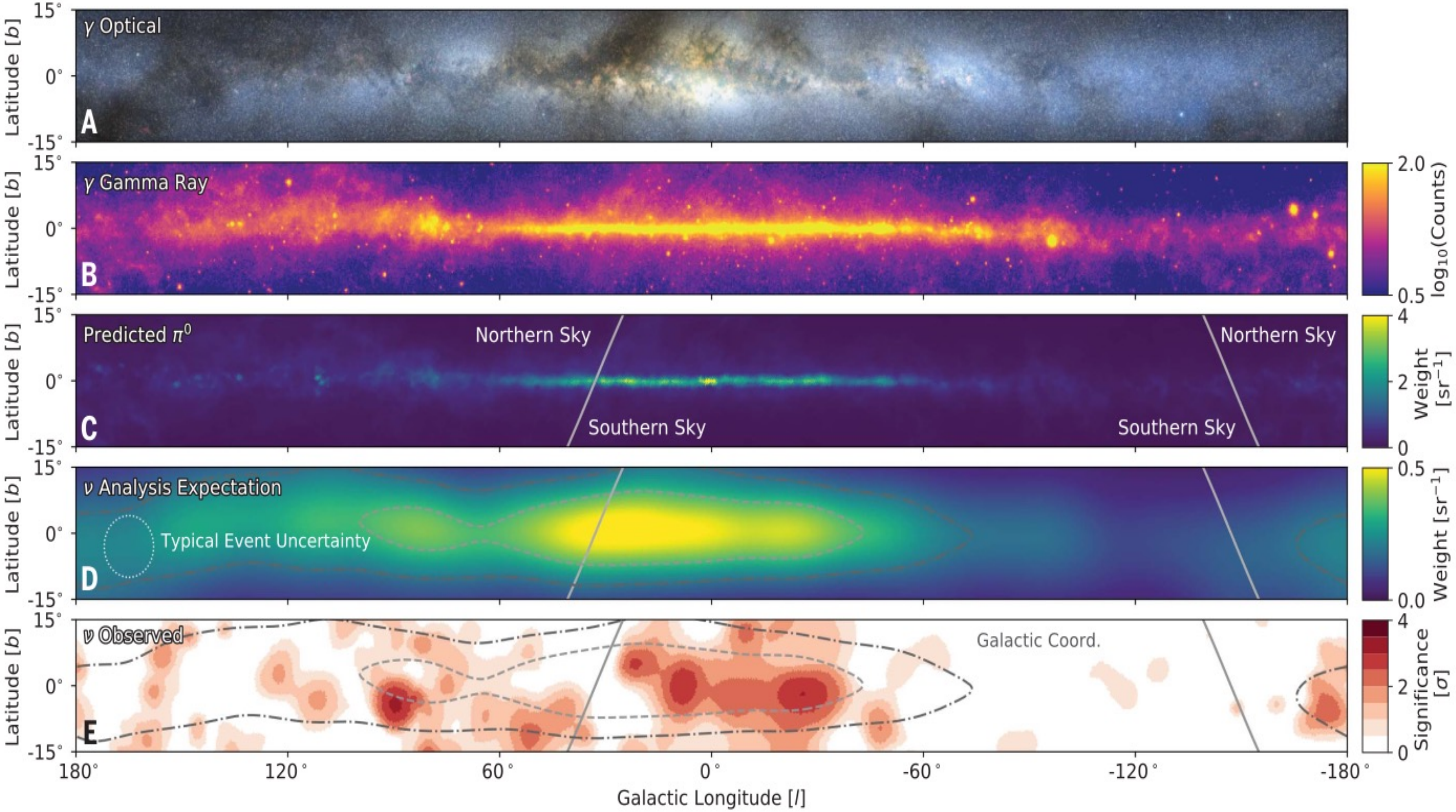

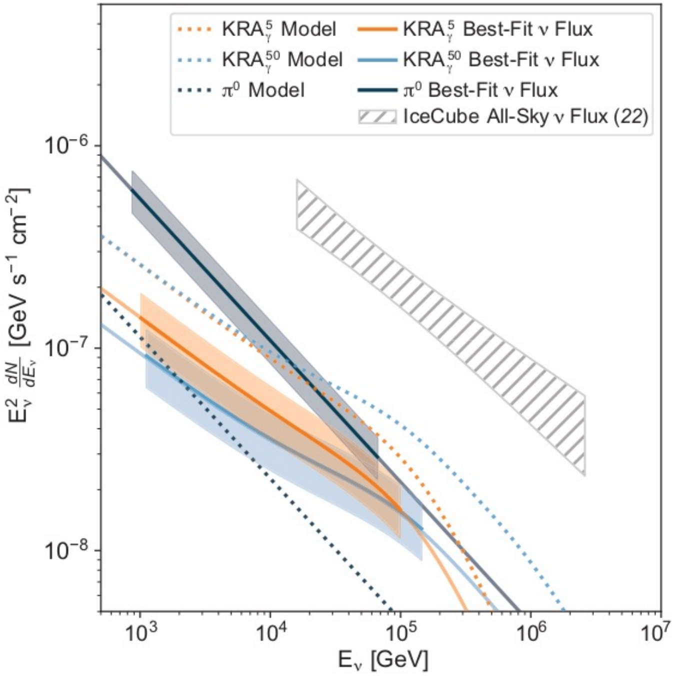

$$E_\gamma^2 \phi_{E_\gamma} \approx 2 E_\nu^2 \phi_{E_\nu}|_{E_\nu = E_\gamma/2}$$

IceCube Collaboration 2023, Science

Neutrino flux: Source v.s. Diffuse

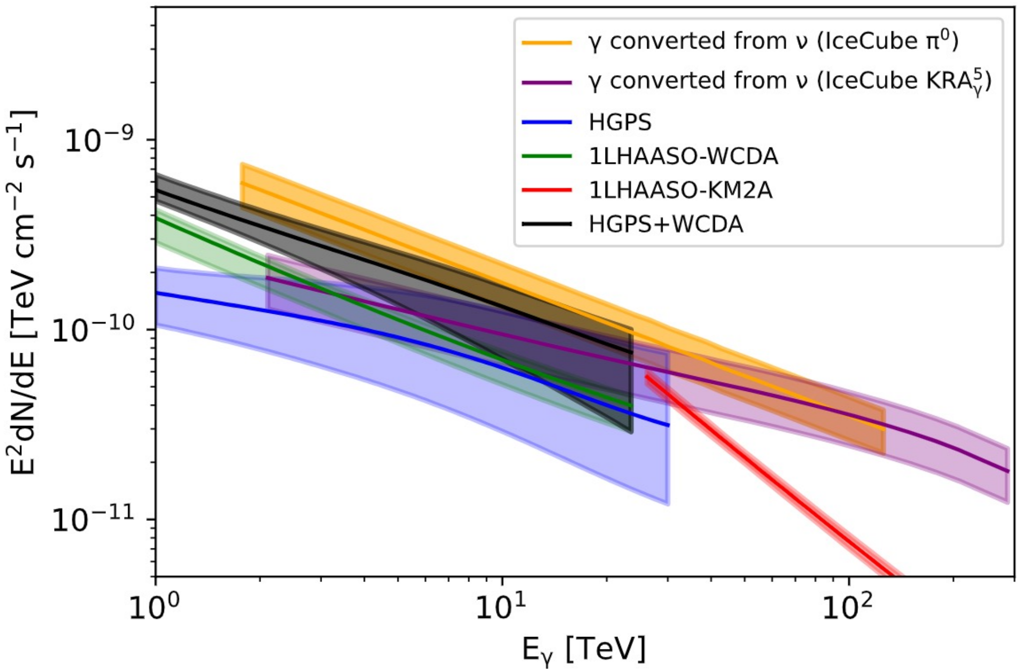

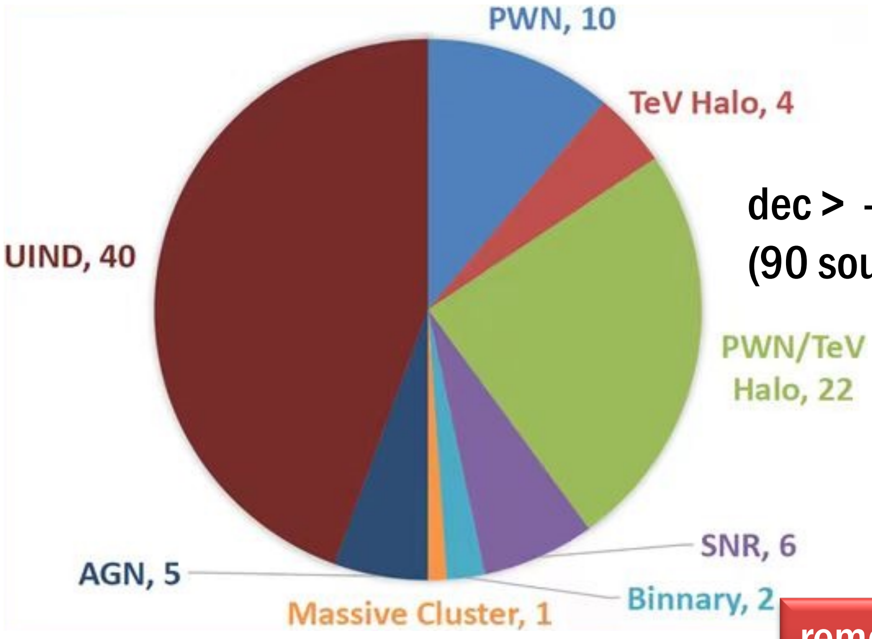

dec > -20, 1LHAASO catalog (90 sources)

removing pulsar-associated sources from the list

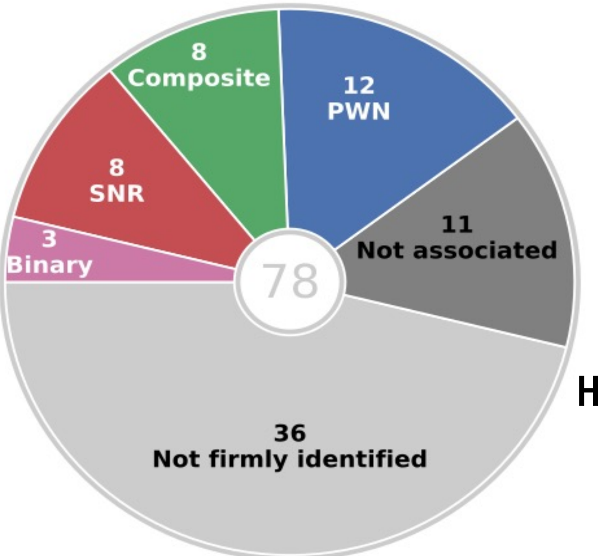

dec < -20, HESS Galactic Plane Survey (78 sources)

HESS Collaboration 2018, A&A

around 10TeV: candidate sources contribute 2/3 total flux (considering systematic error: 1/4 - 1)

above 100TeV: source contribution is negligible

re-scaling the flux

some emission from ISM is also masked

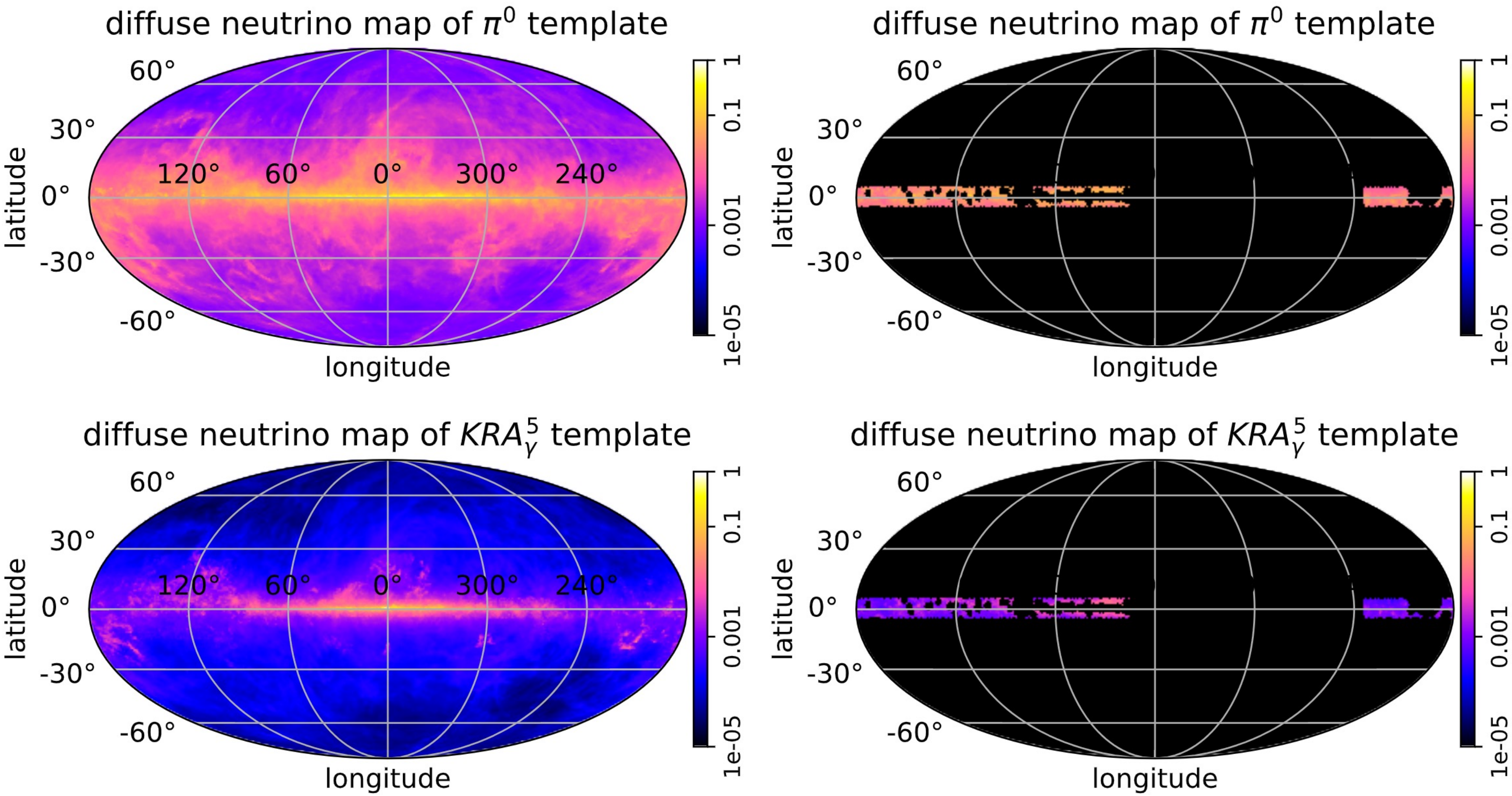

remaining flux

12%

8%

re-scaling the flux

some emission from ISM is also masked

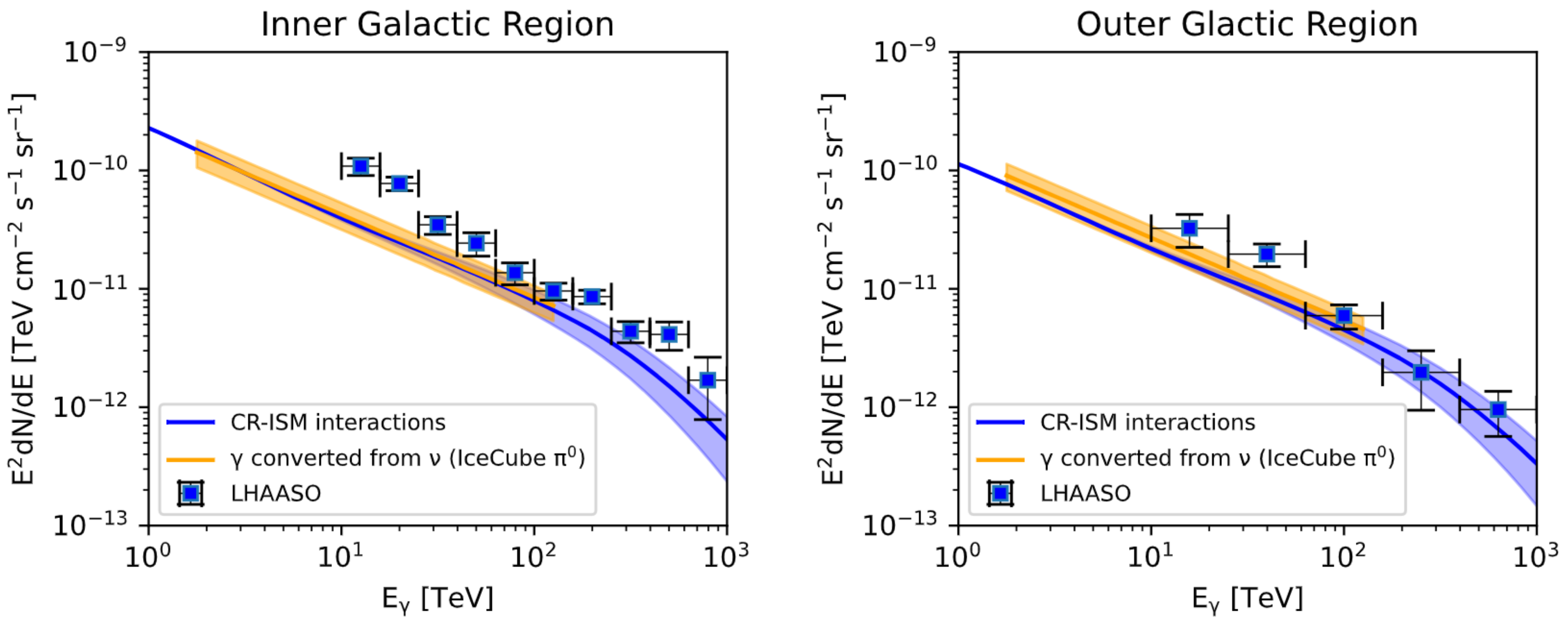

PWN/Pulsar Halos as Extended VHE/UHE gamma-ray sources

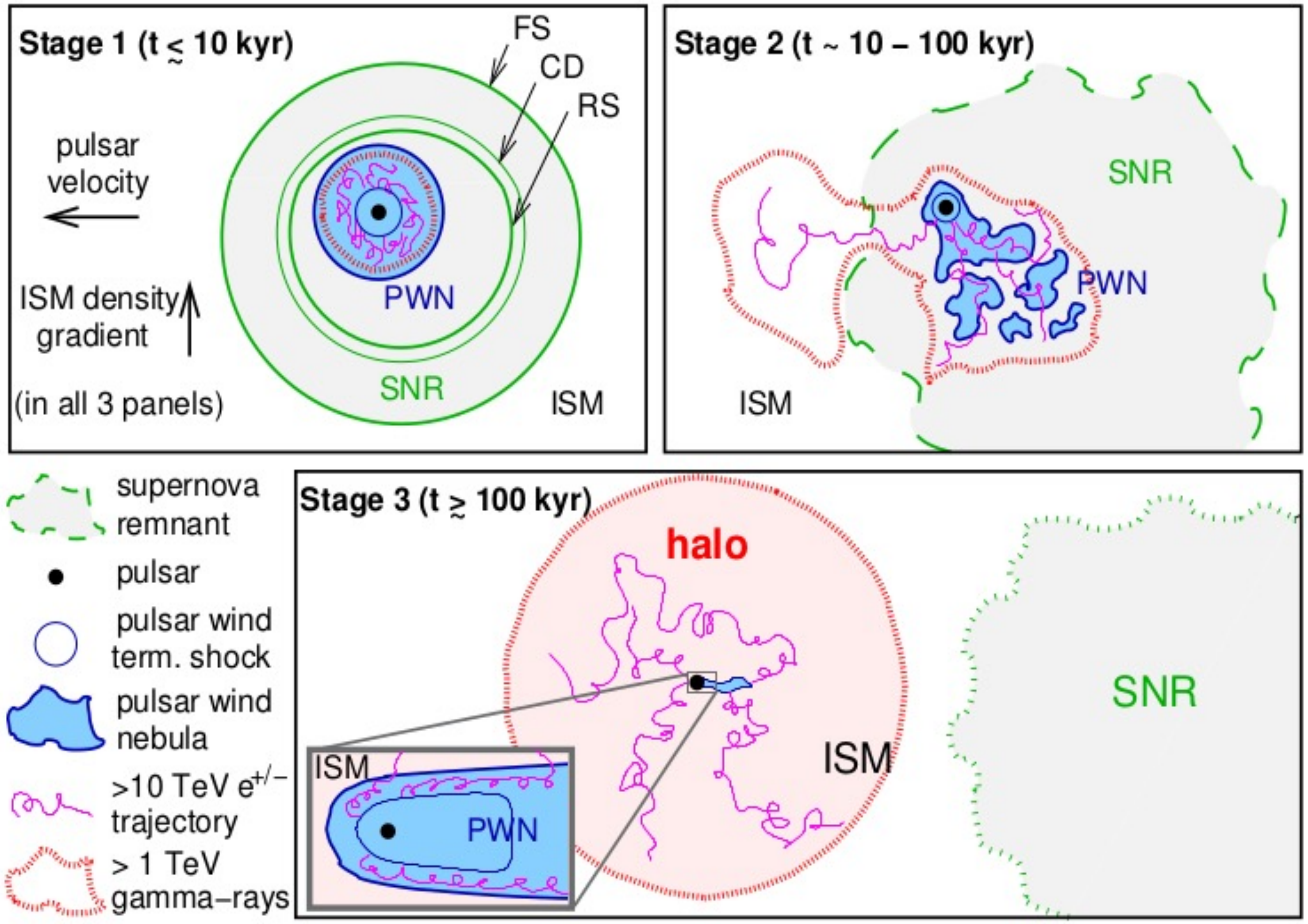

Giacinti et al. 2020, A&A

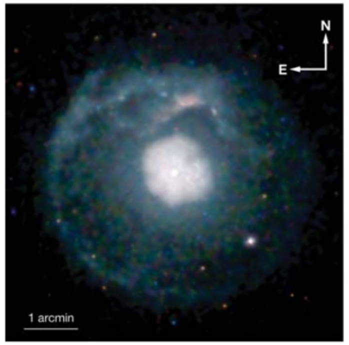

SNR G21.5-0.9
PSR J1833-1034

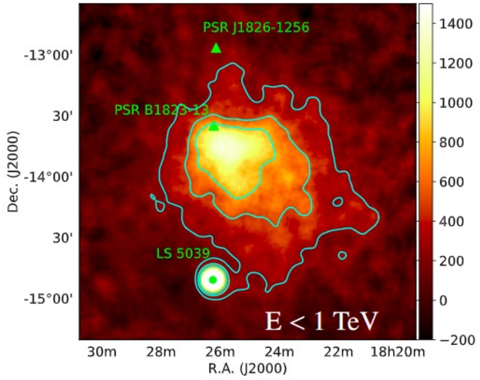

HESS J1825-137
PSR J1826-1334

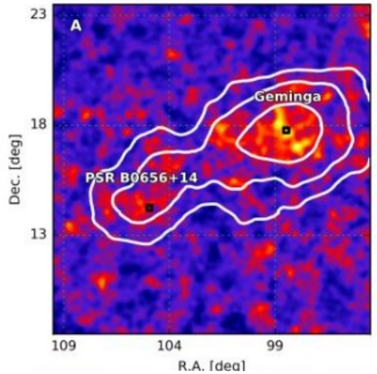

Geminga
Monogem

Discovery of Pulsar Halos

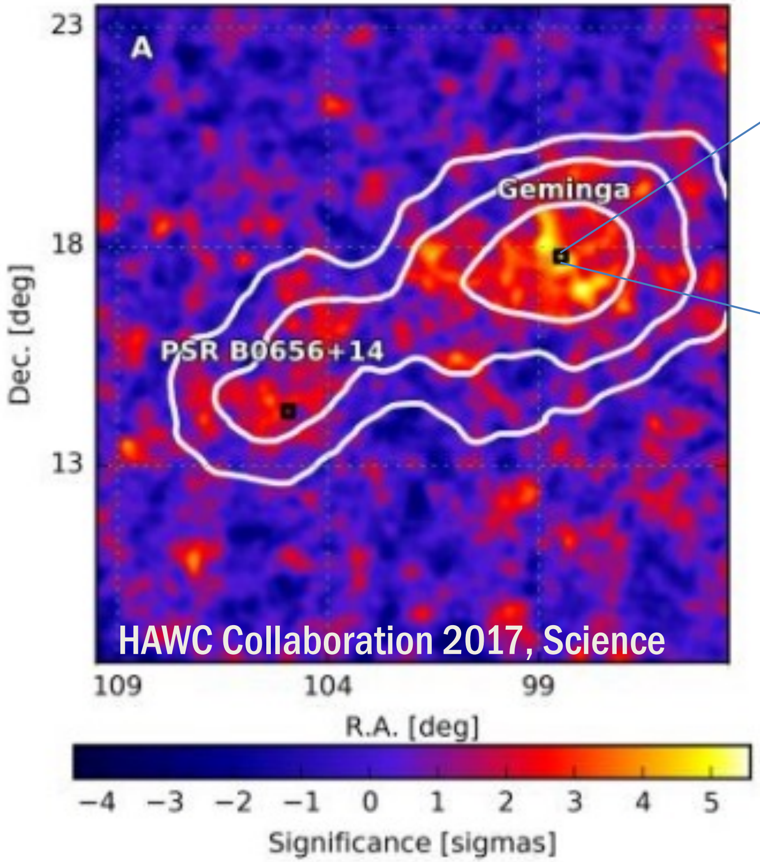

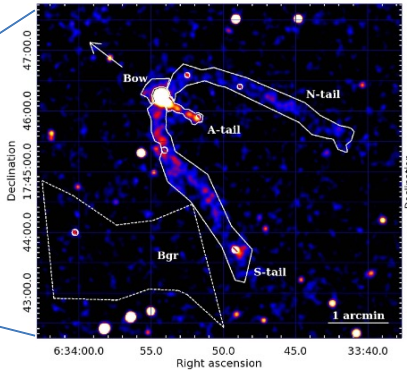

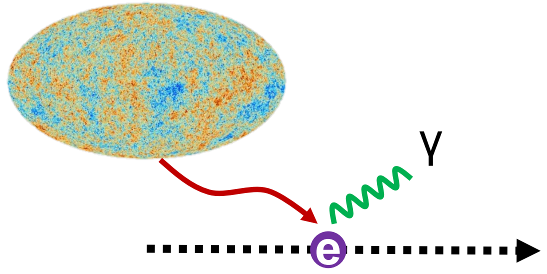

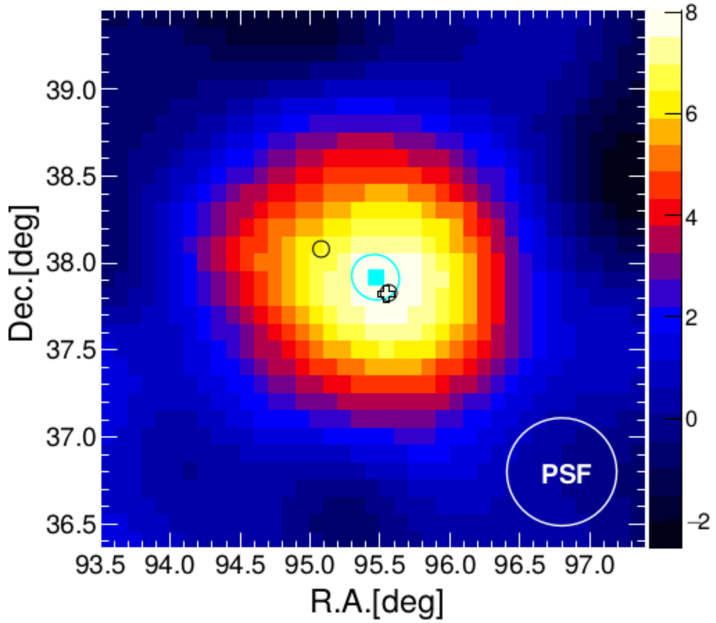

LHAASO Collaboration 2021, PRL

D_{100} (Diffusion coefficient of 100TeV electrons from joint fit of two PWNe)	[$\times 10^{27}$ cm^2/sec]	4.5 ± 1.2

candidates

Source	J0359+5406	J0542+2311	J0634+1741	J1740+0948	J1912+1014	J1914+1150	J2028+3352
PSR	J0359+5414	J0543+2329	J0633+1746	J1740+1000	J1913+1011	J1915+1150	J2028+3332
Age (kyr)	75	253	342	114	169	116	576

Three models for pulsar halos

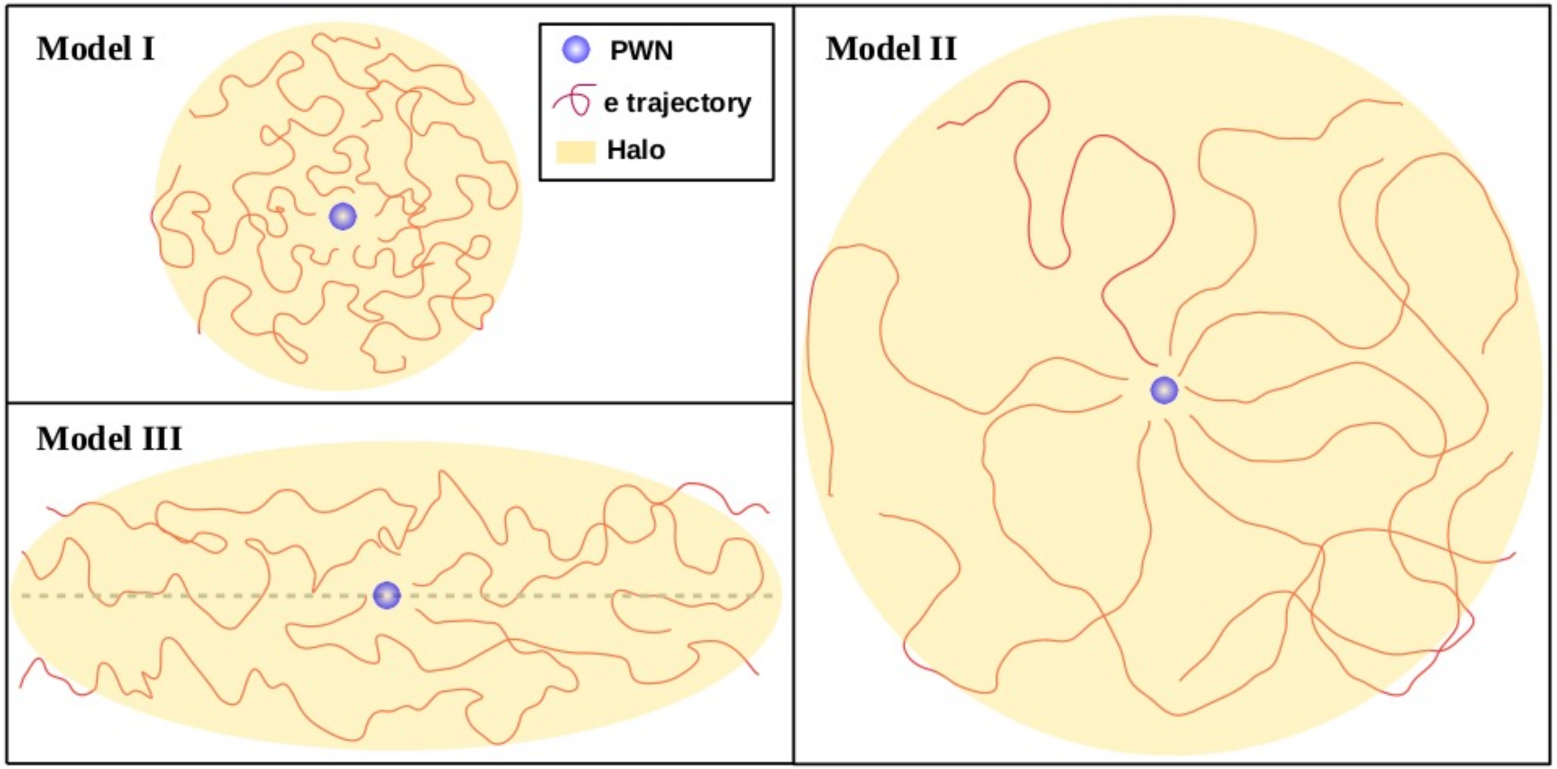

Model	Diffusion coefficient	Magnetic field	Field topology	Energy budget
I	$\sim 0.01 D_{\rm ISM}$	$< 1\,\mu$G	Chaotic	$\sim 0.01 - 0.1 L_s$
II	$\sim D_{\rm ISM}$	$< 1\,\mu$G	Chaotic[a]	$\sim L_s$
III	$D_{\parallel} \sim D_{\rm ISM},\ D_{\perp} \sim 0.01 D_{\rm ISM}$	typical $B_{\rm ISM}$	Regular[b]	$\sim 0.01 - 0.1 L_s$

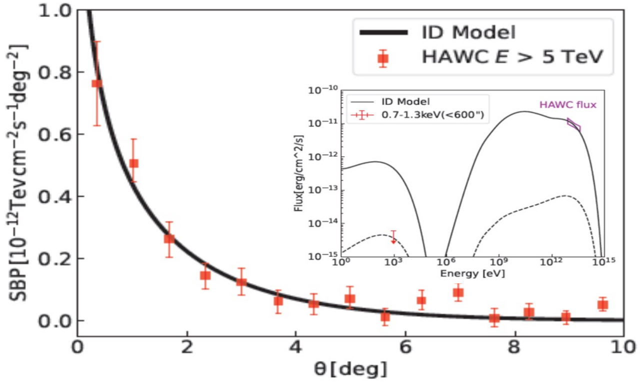

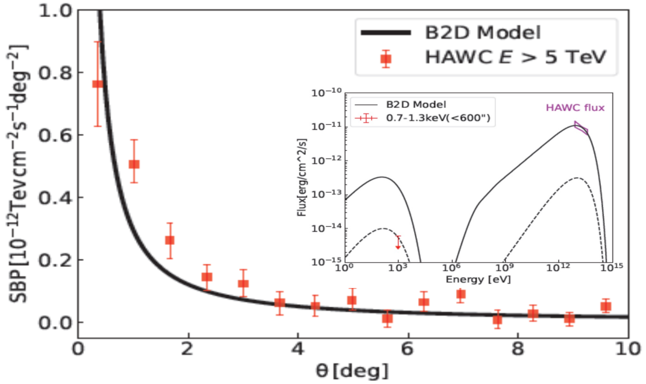

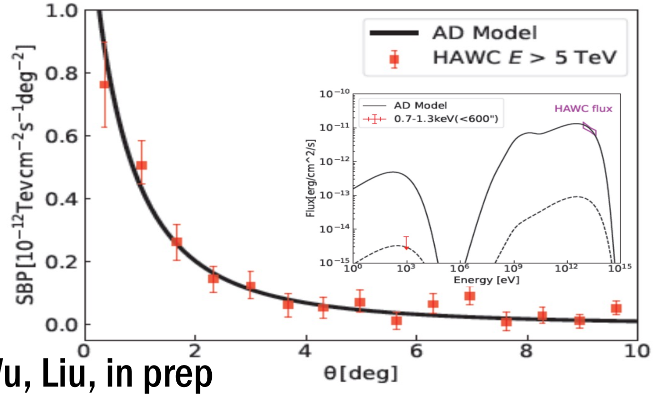

Wu, Liu, in prep

Pulsar Halos as sources of DGE

Pulsar halos : large amount (0.01-0.02/yr), extended (hard to resolve)

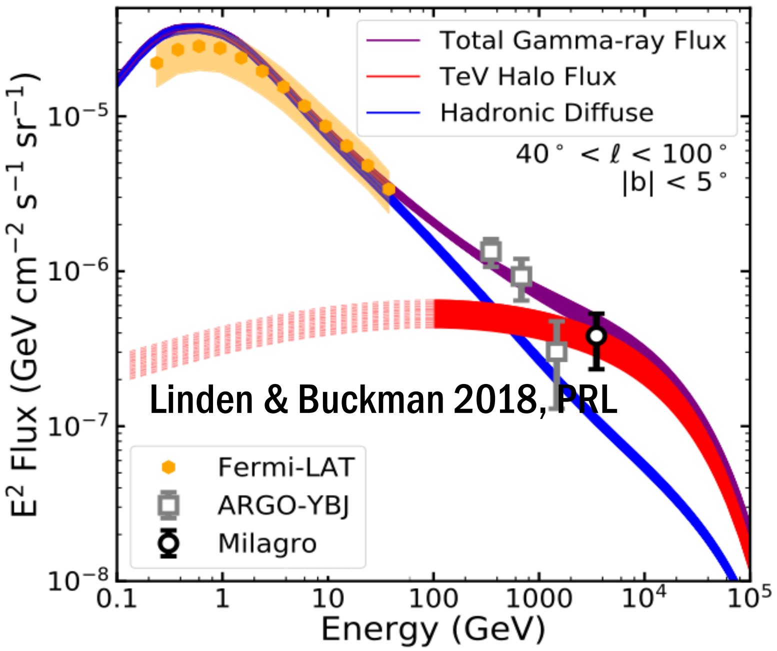

Linden & Buckman 2018, PRL

Simulation of a pulsar sample

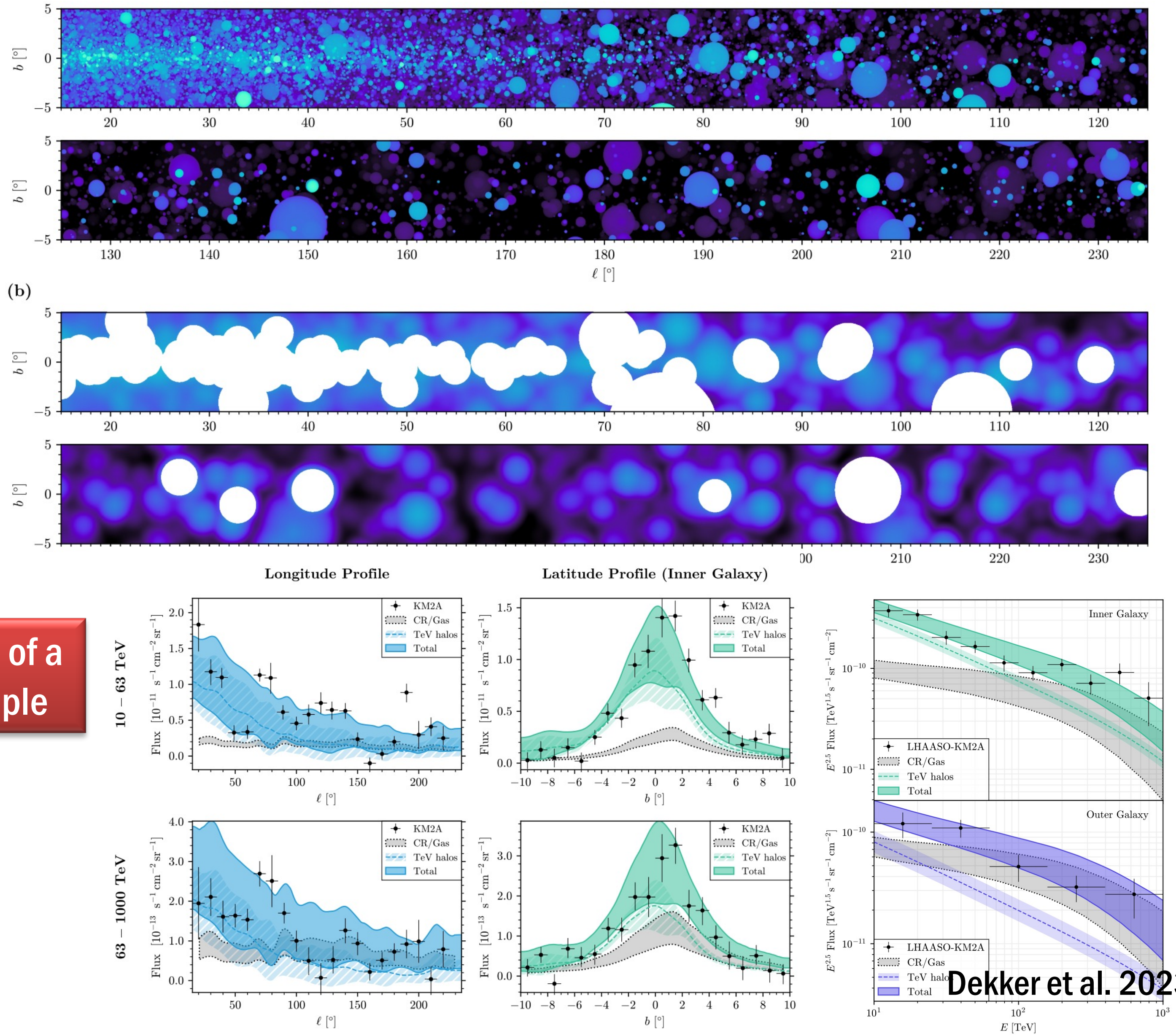

Dekker et al. 2023

pulsar generation at a rate of 0.015/yr

10% of the spin-down power e pairs above 1 GeV

Injection: PL+exp.cutoff, p=1.7, E_c=100TeV

P_0=0.3s, σ_p=0.15s

Simulation with a realistic pulsar sample

- Search in the ATNF puslar catalog, single out pulsars with characteristic age between 50 kyr and 10 Myr (1179)
- Obtain positions of pulsars in the Galaxy with l, b, d
- Generate magnetic field and radiation field around each pulsar
- Simulate pulsar halos powered by these pulsars based on different transport models
- Project each halo onto the celestial sphere
- Mask and calculate the remaining flux
- Correct for contribution of off-beamed pulsars

JName	l [°]	b [°]	P [s]	$\dot{P}$ [s/s]	L_s [erg s^{-1}]	d [kpc]
J1820-0427	25.46	4.73	0.598082	6.33e-15	1.17e+33	2.857
J1821-0331	26.39	4.98	0.902316	2.53e-15	1.36e+32	7.556
J1829+0000	30.46	4.82	0.199147	5.25e-16	2.62e+33	4.353
J1830-0131	29.16	3.99	0.152512	2.11e-15	2.34e+34	3.502
J1832+0029	31.25	4.36	0.533918	1.55e-15	4.03e+32	1.120
J1833-0209	28.92	3.09	0.291931	2.75e-15	4.37e+33	13.360
J1833-0338	27.66	2.27	0.686733	4.16e-14	5.07e+33	2.500
J1833-0559	25.51	1.32	0.483459	1.23e-14	4.31e+33	6.827
J1834-0602	25.64	0.97	0.487914	1.83e-15	6.21e+32	6.340
J1835-0349	27.68	1.86	0.841865	3.06e-15	2.02e+32	5.510
J1835-0600	25.76	0.83	2.221787	8.43e-15	3.03e+31	10.644
J1836-0436	27.17	1.13	0.354237	1.66e-15	1.48e+33	4.358
J1836-0517	26.51	0.92	0.457245	1.30e-15	5.38e+32	8.315
J1837-0045	30.67	2.75	0.617037	1.68e-15	2.83e+32	3.145
J1837-0559	26.00	0.38	0.201064	3.31e-15	1.61e+34	4.315
J1839-0141	30.01	1.97	0.933266	5.94e-15	2.89e+32	6.074
J1839-0223	29.50	1.46	1.26679	4.76e-15	9.25e+31	6.088
J1839-0321	28.60	1.10	0.238782	1.25e-14	3.63e+34	7.852
J1839-0332	28.46	0.93	2.675682	4.76e-15	9.81e+30	4.042
J1839-0402	28.02	0.73	0.52094	7.69e-15	2.15e+33	4.231
J1839-0436	27.41	0.65	0.149461	8.1e-16	9.57e+33	4.483

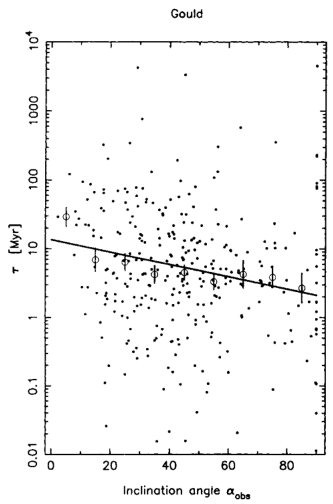

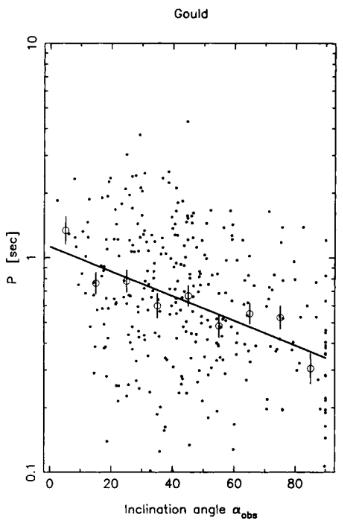

$$f = 9\left(\log\frac{P}{10}\right)^2 + 3,$$

$$f = 1.1\left(\log\frac{\tau}{100}\right)^2 + 15,$$

Tauris & Manchester 1998, MNRAS

Galactic Magnetic field Model

regular component

Field	Best fit Parameters	Description
Disk	$b_1 = 0.1 \pm 1.8\,\mu$G	field strengths at $r = 5$ kpc
	$b_2 = 3.0 \pm 0.6\,\mu$G	
	$b_3 = -0.9 \pm 0.8\,\mu$G	
	$b_4 = -0.8 \pm 0.3\,\mu$G	
	$b_5 = -2.0 \pm 0.1\,\mu$G	
	$b_6 = -4.2 \pm 0.5\,\mu$G	
	$b_7 = 0.0 \pm 1.8\,\mu$G	
	$b_8 = 2.7 \pm 1.8\,\mu$G	inferred from $b_1, ..., b_7$
	$b_{\rm ring} = 0.1 \pm 0.1\,\mu$G	ring at 3 kpc $< r <$ 5 kpc
	$h_{\rm disk} = 0.40 \pm 0.03$ kpc	disk/halo transition
	$w_{\rm disk} = 0.27 \pm 0.08$ kpc	transition width
Toroidal halo	$B_{\rm n} = 1.4 \pm 0.1\,\mu$G	northern halo
	$B_{\rm s} = -1.1 \pm 0.1\,\mu$G	southern halo
	$r_{\rm n} = 9.22 \pm 0.08$ kpc	transition radius, north
	$r_{\rm s} > 16.7$ kpc	transition radius, south
	$w_{\rm h} = 0.20 \pm 0.12$ kpc	transition width
	$z_0 = 5.3 \pm 1.6$ kpc	vertical scale height
X halo	$B_{\rm X} = 4.6 \pm 0.3\,\mu$G	field strength at origin
	$\Theta^0_{\rm X} = 49 \pm 1^\circ$	elev. angle at $z = 0, r > r^c_{\rm X}$
	$r^c_{\rm X} = 4.8 \pm 0.2$ kpc	radius where $\Theta_{\rm X} = \Theta^0_{\rm X}$
	$r_{\rm X} = 2.9 \pm 0.1$ kpc	exponential scale length
striation	$\gamma = 2.92 \pm 0.14$	striation and/or $n_{\rm cre}$ rescaling

Jansson & Farrar 2012a, b

random component

Field	Best fit Parameters	Description
Disk component	$b_1 = 10.81 \pm 2.33\,\mu$G	field strengths at $r = 5$ kpc
	$b_2 = 6.96 \pm 1.58\,\mu$G	
	$b_3 = 9.59 \pm 1.10\,\mu$G	
	$b_4 = 6.96 \pm 0.87\,\mu$G	
	$b_5 = 1.96 \pm 1.32\,\mu$G	
	$b_6 = 16.34 \pm 2.53\,\mu$G	
	$b_7 = 37.29 \pm 2.39\,\mu$G	
	$b_8 = 10.35 \pm 4.43\,\mu$G	
	$b_{\rm int} = 7.63 \pm 1.39\,\mu$G	field strength at $r < 5$ kpc
	$z_0^{\rm disk} = 0.61 \pm 0.04$ kpc	Gaussian scale height of disk
Halo component	$B_0 = 4.68 \pm 1.39\,\mu$G	field strength
	$r_0 = 10.97 \pm 3.80$ kpc	exponential scale length
	$z_0 = 2.84 \pm 1.30$ kpc	Gaussian scale height
Striation	$\beta = 1.36 \pm 0.36$	striated field $B^2_{\rm stri} \equiv \beta B^2_{\rm reg}$

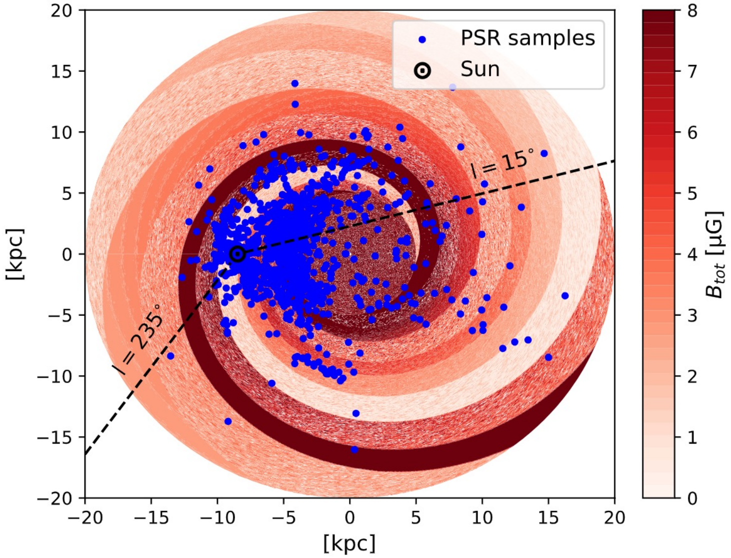

Morphology of individual pulsar halo

AnIsotropic Diffusion Model

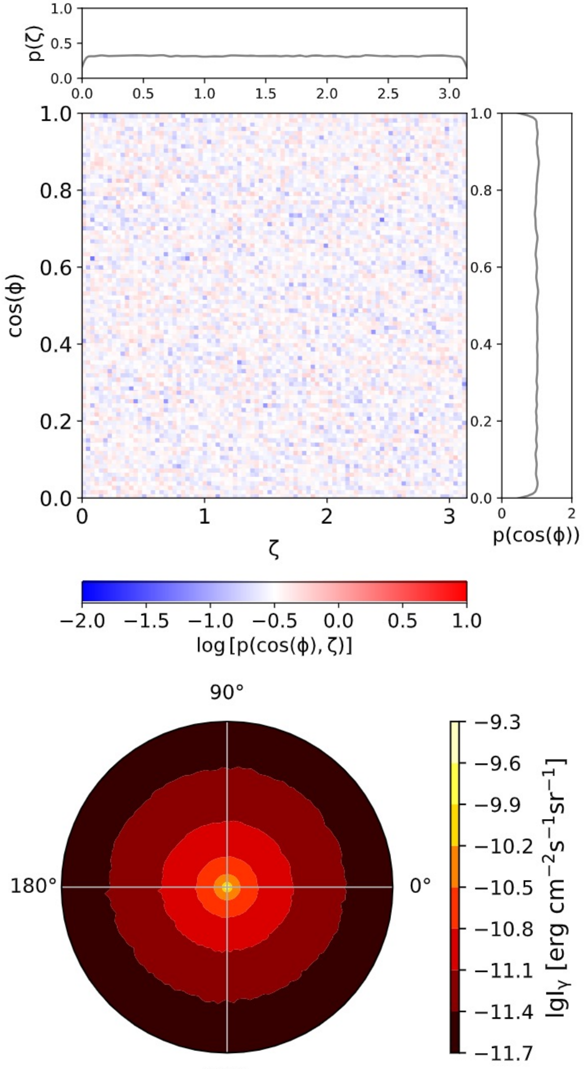

dominated by random field

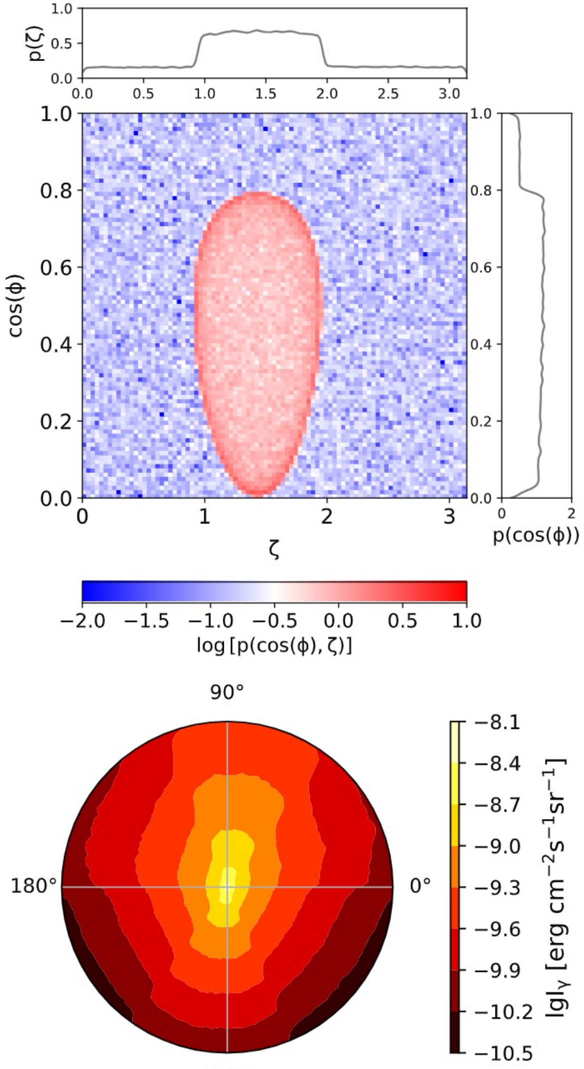

dominated by regular field

$$\frac{\partial N}{\partial t} = \nabla \cdot (\boldsymbol{\mathcal{D}} \cdot \nabla N) - \frac{\partial}{\partial E_e}\left(\dot{E}_e N\right) + Q$$

transport equation in real space and energy space

$$D_{zz} = D_{\parallel} = D_0(E_e/1\mathrm{GeV})^q$$
$$D_{rr} = D_{\perp} = D_{zz} M_A^4 \quad (M_A\text{=0.1-1})$$

Isotropic Diffusion Model

$$D(E,r) = \begin{cases} D_0(E/100\,\mathrm{TeV})^{1/3}, & r < r_b, \\ D_{\mathrm{ISM}}(E/100\,\mathrm{TeV})^{1/3}, & r \geq r_b. \end{cases}$$

r_b = 20 pc

D_0 = 4.5 × 10^{27} cm^{2}s^{-1}

D_{ISM} = 1.8 × 10^{30} cm^{2}s^{-1}

2D Intensity Map

Isotropic Diffusion

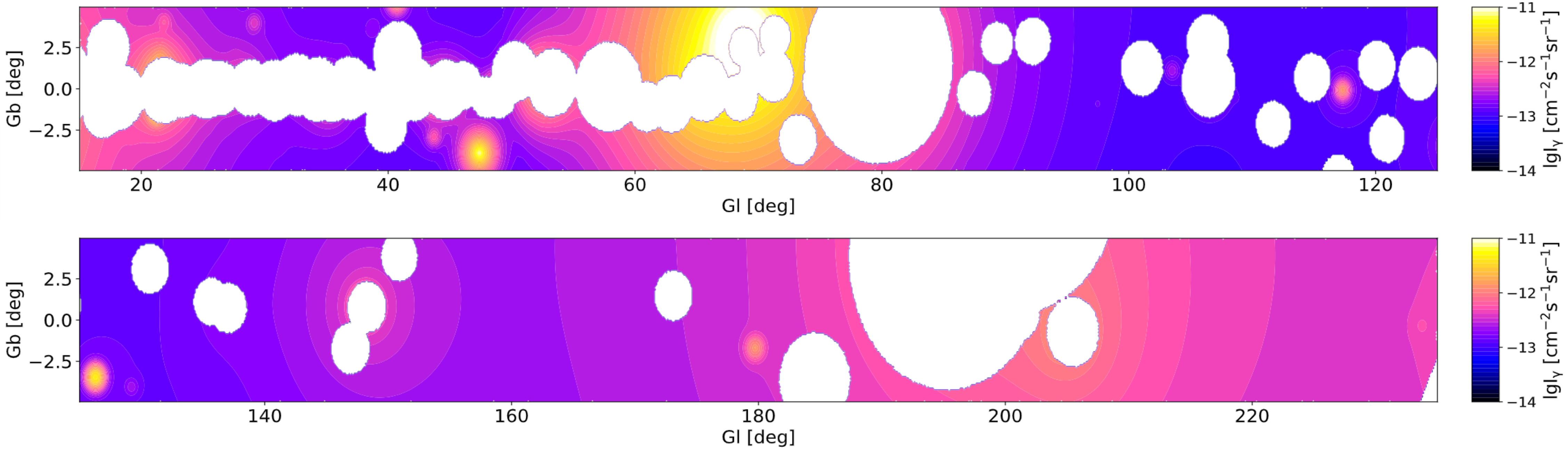

Anisotropic Diffusion

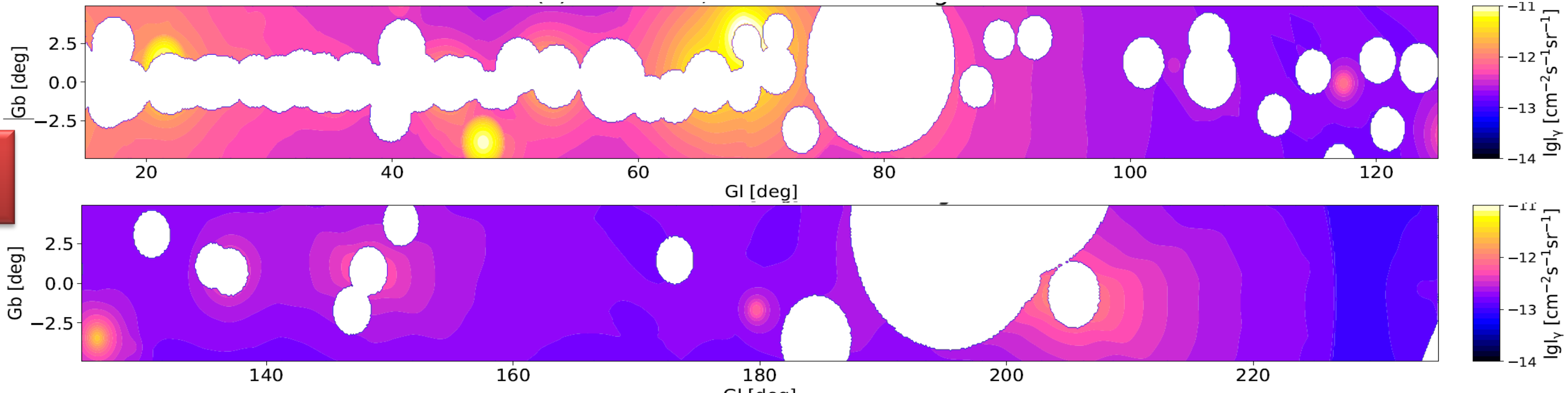

Flux and longitudinal profile

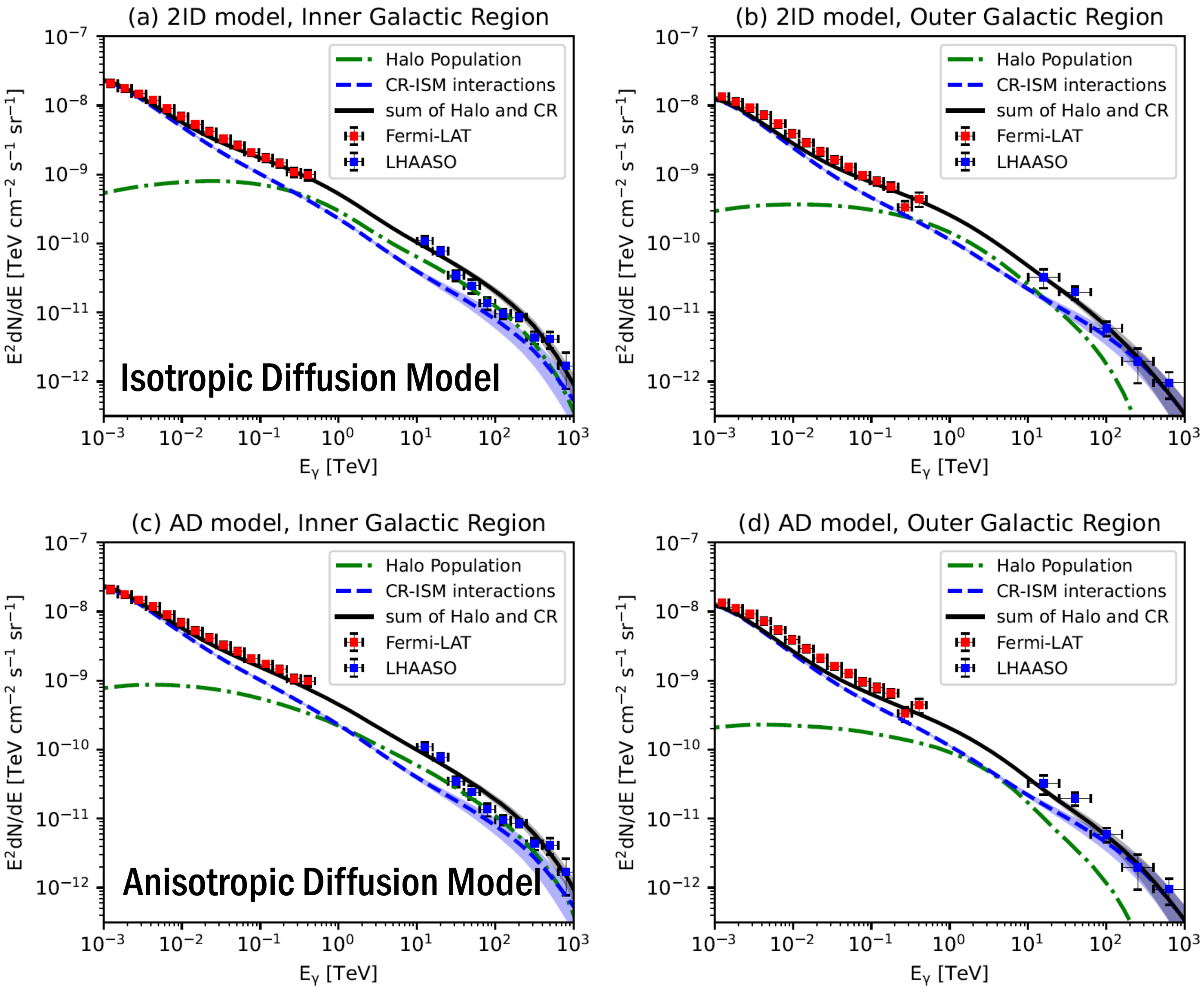

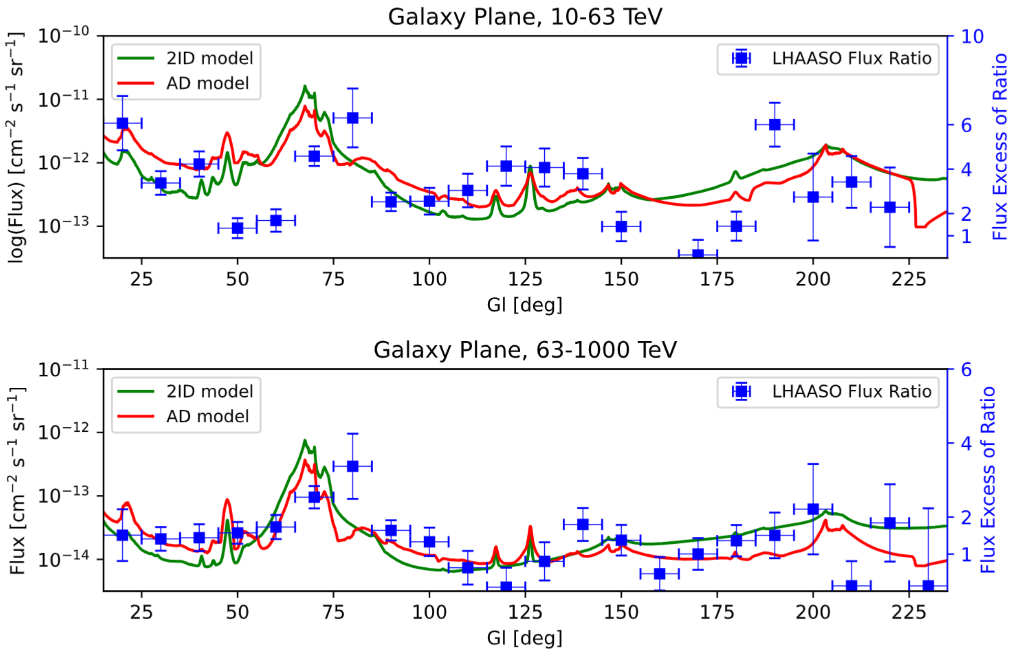

$$Q(E_e, t) = Q_0(t) E_e^{-s} e^{-E_e/E_{max}}$$

$$L_s(t) = \eta_e L_{s,0}/(1+t/\tau_0)^2$$

s=2.2, η_e~0.1 for both models

Yan, Liu et al. 2023, arXiv:2307.12363

Summary

- 10-1000 TeV DGE measured by LHAASO exceeds the prediction of standard CR transport model below 100 TeV
- By comparing the Galactic neutrino flux measured by IceCube and gamma-ray flux of Galactic sources, we found that 2/3 of the measured neutrino flux may originate from hadronic sources and 1/3 from ISM
- There possibly exists a leptonic component in the DGE measured by LHAASO between 10-100 TeV. Beyond 100 TeV, the flux is largely hadronic.
- We modeled the gamma-ray sky arising from pulsar halos based on the measured pulsar sample, and models of Galctic magnetic field and radiation field under both ID model and AD model.
- Pulsar halos may account for the 10-100 TeV excess in DGE (with a possible extension down to ~100GeV)

Thank you for your attention!